



Pergamon

SCIENCE @ DIRECT®

Bioorganic & Medicinal Chemistry Letters 13 (2003) 1469–1474

BIOORGANIC &
MEDICINAL
CHEMISTRY
LETTERS

Structure-Based Design of Inhibitors of Human L-Xylulose Reductase Modelled Into the Active Site of the Enzyme

Vincenzo Carbone,^a Connie Darmanin,^a Shuhei Ishikura,^b Akira Hara^b
and Ossama El-Kabbani^{a,*}

^a*Department of Medicinal Chemistry, Victorian College of Pharmacy, Monash University, 381 Royal Parade, Parkville, Victoria 3052, Australia*

^b*Laboratory of Biochemistry, Gifu Pharmaceutical University, Mitahora-higashi, Gifu 502-8585, Japan*

Received 4 November 2002; accepted 3 February 2003

Abstract—The program GRID was used to design potential inhibitors of human L-xylulose reductase based on a model of the holoenzyme in complex with *n*-butyric acid. The inclusion of phosphate or carboxylate functional groups in the ligand suggested an increase in the net binding energy of the complex up to 2.8- and 4.0-fold, respectively. This study may be useful in the development of potent and specific inhibitors of the enzyme.

© 2003 Elsevier Science Ltd. All rights reserved.

L-Xylulose reductase (XR: EC 1.1.1.10) catalyses the NADPH-linked reduction of L-xylulose to xylitol in the glucuronic acid pathway.¹ This pathway accounts for about 5% of the total glucose catabolized per day in humans,² and the utilization of glucose via this pathway is increased in diabetic rats³ and humans.⁴ Recently, XR has been shown to be localized in the brush-border membranes of proximal tubular cells of mouse kidneys, and suggested to play a role in water reabsorption and cellular osmoregulation by producing xylitol.⁵ The enzymes of the glucuronic acid pathway are also present in mammalian lens, and the flux of sugars and xylitol through this pathway has been suggested to be involved in the osmoregulation processes of the lens and the aetiology of sugar cataracts.⁶ Therefore, potent and specific inhibitors of XR are useful to test the proposed roles of the enzyme, as well as to facilitate the elucidation of the structure-function relationship of the enzyme.

Biochemical studies of XRs in human and rodent tissues⁵ have revealed that the enzyme is a tetramer (composed of 26 kDa subunits), belongs to the short-chain

dehydrogenase/reductase superfamily,⁷ and is competitively inhibited by *n*-butyric acid which binds to the enzyme-NADP⁺ complex (IC₅₀ = 52 μM). Site-directed mutagenesis study shows essential roles of Ser136 and Tyr149 residues in the catalytic function of the enzyme, and suggests possible involvement of several residues in binding of the substrate and *n*-butyric acid.⁸

XR displays a high sequence identity (67%) with mouse lung carbonyl reductase (MLCR),⁹ a member of the short-chain dehydrogenase/reductase superfamily. Sequence alignment of human XR and MLCR carried out using the Clustalw1.60 sequence alignment program¹⁰ is shown in Figure 1. MLCR is a tetramer and its tertiary structure has been determined by X-ray crystallography¹¹ and therefore, for this study a model of XR was constructed based on the MLCR tertiary structure. The modelling program TURBO-FRODO version 5.5¹² was used to replace residues of MLCR with corresponding residues in the human XR sequence, conserving the original secondary structure, followed by an initial energy minimisation using the conjugate gradient method in the program X-PLOR¹³ to relieve any steric strain associated with the atomic coordinates. The program DOCK (version 4.0)¹⁴ was used to position the *n*-butyric acid molecule in favourable orientations in the active site of XR. SPHGEN, a program supplied with DOCK, was used to identify where ligand atoms may be

*Corresponding author. Tel.: +61-3-9903-9691; fax: +61-3-9903-9582; e-mail: ossama.el-kabbani@vcp.monash.edu.au

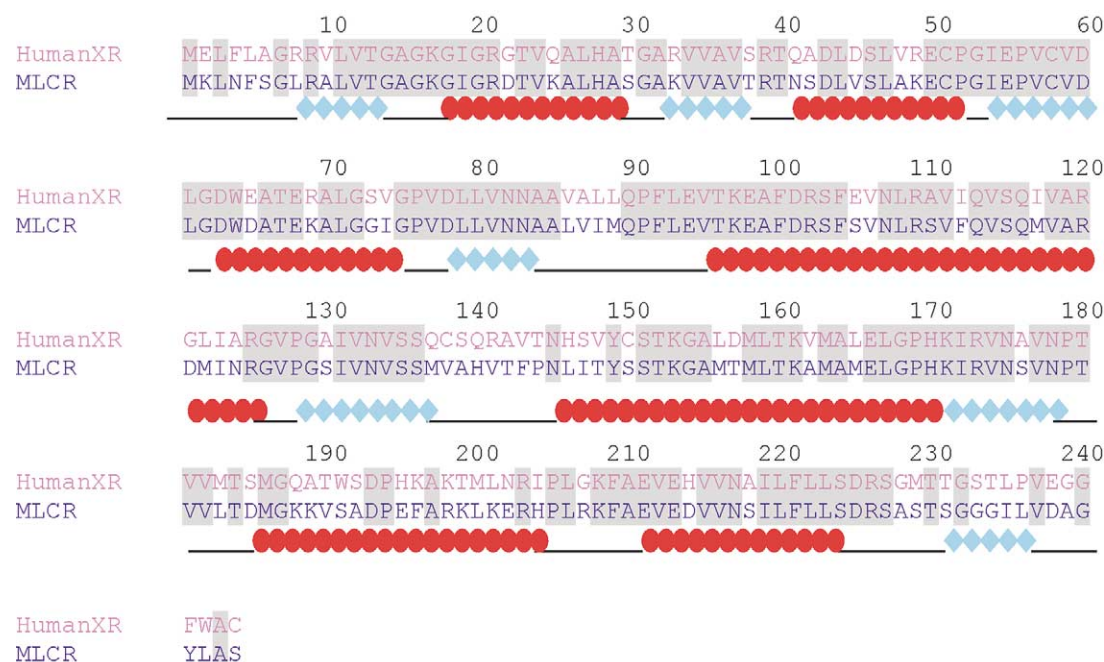


Figure 1. Amino acid sequence alignment of human L-xylulose reductase (Human XR) and mouse lung carbonyl reductase (MLCR). The shaded regions indicate residue identity and regions of α -helices and β -stands are designated by the symbols \bullet and \blacklozenge , respectively.

located within the defined active site region. Each orientation of the docked ligand was evaluated based on shape, steric and electrostatic properties of the active site of the enzyme. The orientation with the highest energy score capturing the interactions with the catalytic residues Ser136 and Tyr149 was used for the ternary complex model (Fig. 2). The chosen orientation ranked 8 in a total number of 44 possible orientations and had an energy score of -26.40 compared to a maximum energy score of -27.55 .

The program GRID (version 18)¹⁵ was used to search the active site of the enzyme for the most appropriate positions for a variety of probes, as previously described.¹⁶ Briefly, 25 independent probes which included a variety of functional groups and ions were used to search the active site of XR for their most favourable positions. The corresponding contour maps were visualised using the contour facility of the InsightII package version 2.1 (Biosym Technologies Inc., San Diego, CA USA). Calculations were performed on a sphere (15 \AA

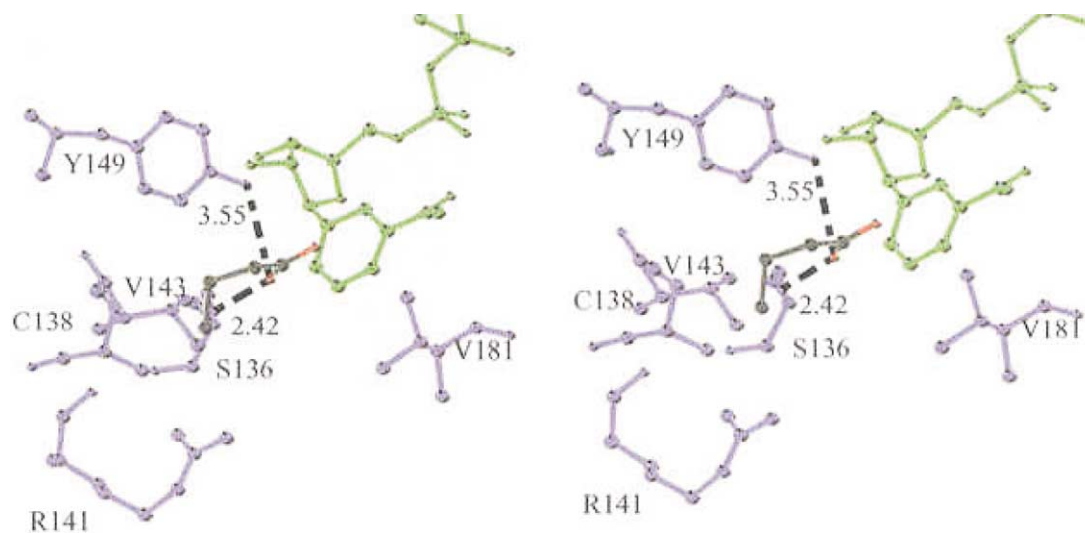


Figure 2. Stereoview of *n*-butyric acid (compound 1, black and red) docked into the active site of human XR. NADP⁺ (green) and residues within 4 Å of compound 1 (blue) are shown. Hydrogen bonds exist between compound 1 and Ser136 OG (2.42 Å) and Tyr149 OH (3.55 Å). The figure was prepared using MOLSCRIPT.¹⁸

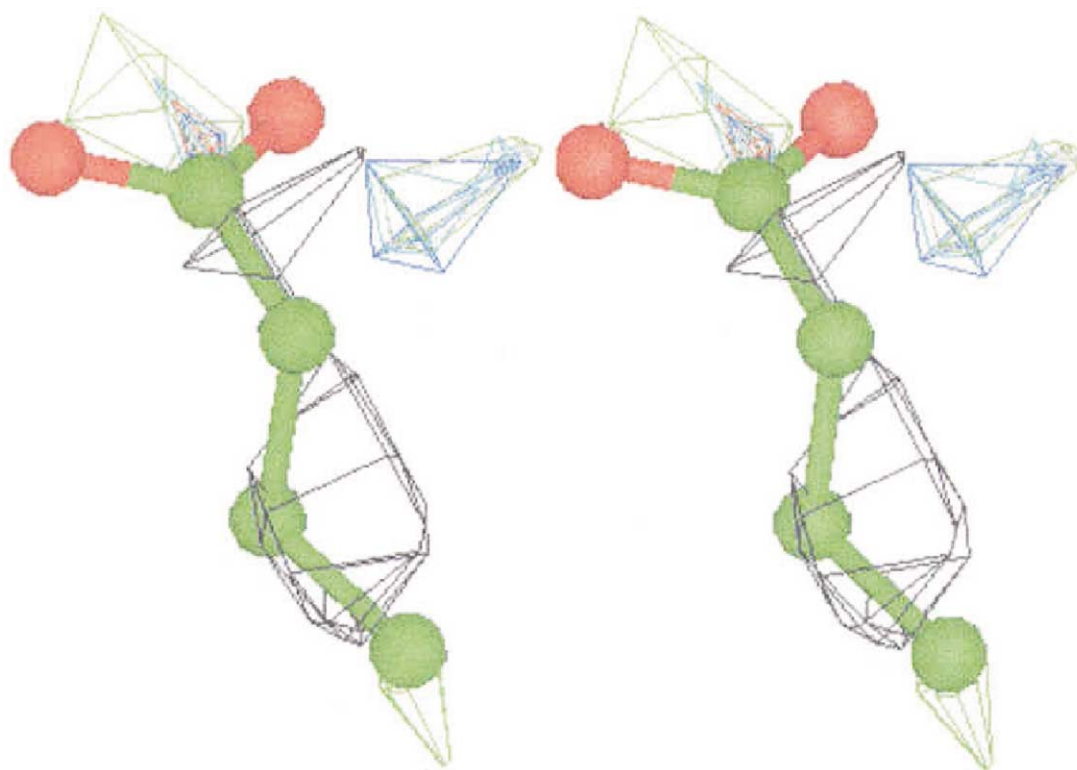


Figure 3. Stereoview showing contours of interaction energies between the active site of XR and phosphate (black), hydroxyl phenyl (grey), hydroxyl (purple), methyl (blue), carboxylate (green) and carbonyl (red) probes with the superimposed *n*-butyric acid (compound **1**). The figure was prepared using InsightII (Biosym Technologies, San Diego, CA, USA).

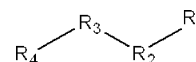
radius) centred on the active site, with a grid spacing of 0.5 Å. The interaction energy between the probe and every atom within the protein structure was evaluated at each grid point. A dielectric constant of 80 was used to simulate a bulk aqueous phase, while areas as determined by GRID to be excluded from the solvent were assigned a dielectric constant of 4 (i.e., the interior of the protein). The accompanying program GRIN was used to automatically assign atom types and charges for the protein using the standard parameter file provided with GRID. The output was converted (using GINS supplied with GRID) into a form suitable for input to the Biosym utility contour. Contour maps were built using steps of 0.4 kcal/mol, where negative energy levels depict regions where ligand binding is most favourable and positive energy levels define the surface of the target. The contour map was then superimposed on the active site of the XR model using InsightII. Superposition of *n*-butyric acid on the active site of XR pro-

vided information on the predicted position of the probes with respect to the *n*-butyric acid molecule as shown in Figure 3. The most favoured probes are listed in Table 1 with the phosphate probe being the most favoured and the carbonyl group the least favoured. The GRID results suggested that the addition of functional groups comprised of the probes listed in Table 1 may improve the binding energies of the complex. The designed compounds were then docked manually in the active site of XR based on the orientation of the modelled *n*-butyric acid (compound **1**) so that each probe would be placed in its corresponding favoured region of interaction.

Energy minimisation and molecular dynamics calculations were carried out on the 11 compounds (general formula shown in Scheme 1) listed in Table 2 using the Discover 2.7 package (Biosym Technologies, San Diego, CA, USA) on an O2 (R12000) workstation (Silicon Graphics, Mountain View, CA, USA) following previously established procedures.^{16,17} Minimisation calculations were initially carried out to relieve any steric hindrance associated with the docked compounds. Calculations were carried out to maximum atomic root-mean-square derivatives of 10.0 and 0.01 kcal/Å using the algorithms steepest descent and conjugate gradient,

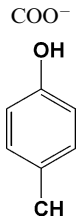
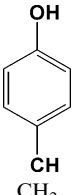
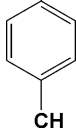
Table 1. GRID analysis results showing the contour energy levels (kcal) within the active site of XR for the best six probes

Probe	Max. energy (kcal)
Phosphate	−12.4
Hydroxyl	−8.7
Carboxylate	−8.4
Hydroxy phenyl	−8.2
Methyl	−8.2
Carbonyl	−6.4



Scheme 1.

Table 2. Protein interaction energies (kcal/mol) calculated between XR residues and compounds **1–11** having the general formula shown in Scheme 1

Compd	Structure				Protein interaction energy (kcal/mol)
	R ₁	R ₂	R ₃	R ₄	
1	COO [−]	CH ₂	CH ₂	CH ₃	−40.44
2	COO [−]	CHCH ₃	CH ₂	CH ₃	−29.16
3	COO [−]	CHOH	CH ₂	CH ₃	−38.36
4	COO [−]	CHCH ₂ OH	CH ₂	CH ₃	−41.42
5	COO [−]	CHCOO [−]	CH ₂	CH ₃	−86.68
6	COO [−]	CH ₂	CH ₂	COO [−]	−113.69
7	COO [−]	CHCOO [−]	CH ₂	COO [−]	−162.54
8			CH ₂	CH ₃	−51.57
9		CH ₂	CH ₂	CH ₃	−26.88
10	PO ₄ ^{3−}	CH ₂	CH ₂	CH ₃	−87.40
11	COO [−]	CH ₂	PO ₄ ^{3−}	CH ₃	−114.30

respectively. To prevent dynamics calculations from being carried out in vacuum and altering significantly the relative positions of the residues, an aqueous environment around the active site was created using the SOAK (15 Å radius) option in InsightII. Molecular dynamics were then performed using the leapfrog algorithms in Discover. Dynamics were equilibrated for 2 ps with time steps of 1 fs and then continued for 4 ps with time steps of 2 fs at 320 K. Finally, the resulting structures were extracted and energy minimised. The calculated binding energies between XR and compounds **1–11** are listed in Table 2.

Molecular dynamics calculations suggested that compounds **2**, **3**, **4** and **9** had no beneficial effect on the net binding energy of the complex when compared to compound **1** (*n*-butyric acid), after taking into account any energy loss that may result from the displacement of water molecules in the active site of the enzyme by the compounds (Table 2). The addition of a carboxylate group to the *n*-butyric acid molecule as R₂ in compounds **5** and **7**, and R₄ in compound **6** produced the most favoured compounds by increasing the net binding energies of the complexes by 2.1-, 4.0- and 2.8-fold, respectively. The relatively high increase in the net binding energies of the complexes resulted from the introduction of new electrostatic interactions between the negatively charged carboxylate groups of the compounds and the side-chains of the polar residues Gln137, Arg141 and Lys196 (Fig. 4). The replacement of the carboxylate of *n*-butyric acid with a phosphate group enhanced the net binding energy of the complex by 2.2-fold (compound **10**), while the addition of a phosphate group as R₃ in compound **11** suggested an increase in the net binding energy by

2.8-fold. Moreover, an addition of a hydroxy phenyl group as R₂ in compound **8** suggested an enhancement in the net binding energy of the complex by 1.3-fold (Table 2).

The enhanced binding energies for the complexes between the XR molecule and compounds **7** (−162.54 kcal/mol) and **11** (−114.30 kcal/mol), compared to *n*-butyric acid (compound **1**; −40.44 kcal/mol), reflected the introduction of new interactions between the active site of the enzyme and the compounds. Similar to the *n*-butyric acid molecule (Fig. 2), compounds **7** and **11** (Fig. 4) were hydrogen bonded to Ser136 OG (2.42 Å, 2.64 Å and 2.49 Å respectively). New hydrogen bonds for compounds **7** and **11** included Arg141 NH1 (3.11 Å and 2.89 Å, respectively), Arg141 NH2 (3.34 Å and 2.60 Å, respectively) and Gln137 NE2 (3.34 Å and 2.61 Å, respectively). Compound **7** formed an additional ionic bond with Lys196 NZ (3.37 Å), suggesting tighter binding between XR and compound **7**.

In conclusion, the addition of a carboxylate group (R₂ in compounds **5** and **7**, and R₄ in compounds **6** and **7**) and a phosphate group (R₁ in compound **10** and R₃ in compound **11**) to the *n*-butyric acid molecule, as suggested by the program GRID, captured new electrostatic interactions with XR, resulting in an increase in the net binding energy of the complex. While the design and modelling of compounds **5**, **6**, **8**, **10** and **11** suggested an increase in the net binding energies of the complexes, our results indicated that compound **7** may form the complex with the maximum net binding energy and may be useful as a starting model in the development of specific inhibitors for XR.

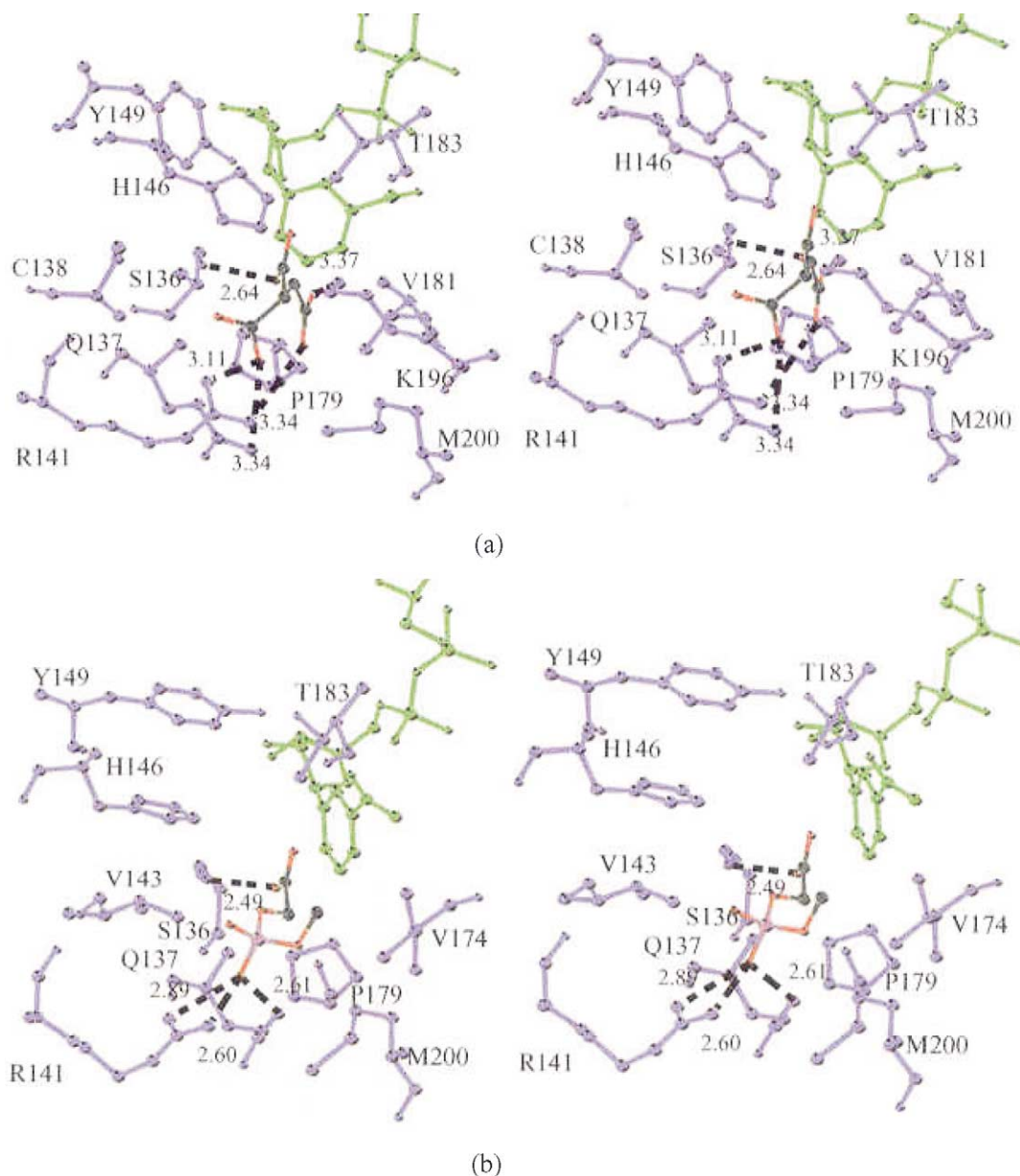


Figure 4. Stereoviews of (a) compound **7** (black and red; R₂=CHCOO⁻, R₄=COO⁻) and (b) compound **11** (black and red; R₃=PO₄³⁻) modelled into the active site of human XR. NADP⁺ (green) and residues (blue) within 4 Å of the compounds are shown. Hydrogen bonds exist between compound **7** and residues Ser136 OG (2.64 Å), Gln137 NE2 (3.34 Å) and Arg141 NH1 and NH2 (3.11 and 3.34 Å, respectively). Hydrogen bonds are shown between compound **11** and residues Ser136 OG (2.49 Å), Gln137 NE2 (2.61 Å), Arg141 NH1 and NH2 (2.89 Å and 2.60 Å, respectively) and Lys196 NZ (3.37 Å). The figures were prepared after molecular dynamics calculations using MOLSCRIPT.¹⁸

References and Notes

1. Touster, O.; Reynolds, V. H.; Hutcheson, R. M. *J. Biol. Chem.* **1954**, *221*, 697.
2. Hollmans, S.; Touster, O. In: *Non-Glycolytic Pathways of Metabolism of Glucose*. New York/London, Academic Press, 1964, pp 107–113.
3. Sochor, M.; Baquer, N. Z.; Mclean, P. *Arch. Biochem. Biophys.* **1979**, *198*, 632.
4. Weingrad, A. I.; Burden, C. L. *New Eng. J. Med.* **1966**, *274*, 298.
5. Nakagawa, J.; Ishikura, S.; Asami, J.; Isaji, T.; Usami, N.; Hara, A.; Sakurai, T.; Tsuritani, K.; Oda, K.; Takahashi, M.; Yoshimoto, M.; Otsuka, N.; Kitamura, K. *J. Biol. Chem.* **2002**, *277*, 17883.
6. Goode, D.; Lewis, M. E.; Crabbe, J. C. *FEBS Lett.* **1996**, *395*, 174.
7. Jörnvall, H.; Persson, B.; Krook, M.; Atrian, S.; Gonzalez-Duarte, R.; Jeffery, J.; Ghosh, D. *Biochemistry* **1995**, *34*, 6003.
8. Ishikura, S.; Isaji, T.; Usami, N.; Nakagawa, J.; El-Kabani, O.; Hara, A. *Chem.-Biol. Interact.* In press.
9. Nakanishi, M.; Deyashiki, Y.; Ohshima, K.; Hara, A. *Eur. J. Biochem.* **1995**, *228*, 381.

10. Thompson, J. D.; Higgins, D. G.; Gibson, T. J. *Nucleic Acids Res.* **1994**, *22*, 4673.
11. Tanaka, N.; Nonaka, T.; Nakanishi, M.; Deyashiki, Y.; Hara, A.; Mitsui, Y. *Structure* **1996**, *4*, 33.
12. Roussel, A.; Fontecilla-Camps, J. C.; Cambillau, C. *Acta Crystallogr. Sect. A* **1990**, *46*, C66.
13. Brünger, A. T.; Krukowski, A.; Erickson, J. W. *Acta Crystallogr. Sect. A* **1990**, *46*, 585.
14. Ewing, T. University of California, CA. 1998, DOCK manual version 4.0.
15. Goodford, P. J. *J. Med. Chem.* **1985**, *28*, 849.
16. Darmanin, C.; El-Kabbani, O. *Bioorg. Med. Chem. Lett.* **2001**, *11*, 3133.
17. Darmanin, C.; El-Kabbani, O. *Bioorg. Med. Chem. Lett.* **2000**, *10*, 1101.
18. Kraulis, P. J. *J. Appl. Cryst.* **1991**, *24*, 946.